

Positional cloning of *Sorcs1*, a type 2 diabetes quantitative trait locus

Susanne M Clee¹, Brian S Yandell^{2,3}, Kathryn M Schueler¹, Mary E Rabaglia¹, Oliver C Richards¹, Summer M Raines¹, Edward A Kabara¹, Daniel M Klass¹, Eric T-K Mui¹, Donald S Stapleton¹, Mark P Gray-Keller¹, Matthew B Young¹, Jonathan P Stoehr¹, Hong Lan¹, Igor Boronenkov¹, Philipp W Raess¹, Matthew T Flowers¹ & Alan D Attie¹

We previously mapped the type 2 diabetes mellitus-2 locus (*T2dm2*), which affects fasting insulin levels, to distal chromosome 19 in a leptin-deficient obese F₂ intercross derived from C57BL/6 (B6) and BTBR T⁺ tf/J (BTBR) mice¹. Introgression of a 7-Mb segment of the B6 chromosome 19 into the BTBR background (strain 1339A) replicated the reduced insulin linked to *T2dm2*. The 1339A mice have markedly impaired insulin secretion *in vivo* and disrupted islet morphology. We used subcongenic strains derived from 1339A to localize the *T2dm2* quantitative trait locus (QTL) to a 242-kb segment comprising the promoter, first exon and most of the first intron of the *Sorcs1* gene. This was the only gene in the 1339A strain for which we detected amino acid substitutions and expression level differences between mice carrying B6 and BTBR alleles of this insert, thereby identifying variation within the *Sorcs1* gene as underlying the phenotype associated with the *T2dm2* locus. SorCS1 binds platelet-derived growth factor, a growth factor crucial for pericyte recruitment to the microvasculature, and may thus have a role in expanding or maintaining the islet vasculature. Our identification of the *Sorcs1* gene provides insight into the pathway underlying the pathophysiology of obesity-induced type 2 diabetes mellitus.

Obesity is a major risk factor for type 2 diabetes mellitus. However, although they are insulin resistant, most obese individuals do not develop diabetes. Type 2 diabetes mellitus results when the pancreas of an insulin-resistant individual is unable to produce sufficient insulin to compensate for the body's increased demand for insulin, for example by expanding β -cell mass or increasing insulin secretion^{2,3}. The molecular determinants of pancreatic compensation are not completely understood, so there are no reliable ways to predict which obese individuals will transition from insulin resistance alone to type 2 diabetes mellitus.

Genetic factors account for approximately 50% of an individual's risk of developing type 2 diabetes mellitus⁴. Many candidate genes for this disease have emerged from studies of insulin resistance and β -cell biology, but few of these genes are associated with the disease, and the search for new type 2 diabetes mellitus genes has met with limited success in human populations^{4–7}. To identify the factors promoting diabetes in obese individuals, we conducted genetic studies on two obese mouse strains differing in diabetes susceptibility.

B6 mice homozygous for the *Lep^{ob}* mutation (B6.ob) have mild fasting hyperglycemia, whereas BTBR mice homozygous for the same mutation (BTBR.ob) are severely diabetic^{1,8}. We mapped loci affecting fasting plasma glucose and insulin levels segregating in these strains in an obese F₂ intercross derived from these two strains¹. This identified the *T2dm2* QTL on chromosome 19, where alleles from the nondiabetic B6 strain are associated with a 30% reduction in fasting plasma insulin levels and a coincident lod peak for increased plasma glucose levels that did not reach the genome-wide significance level¹. To fine-map this locus, we created congenic mice by introgressing segments of B6 chromosome 19 into the BTBR.ob background, predicting that B6 alleles would further reduce the insulin levels of BTBR.ob mice.

The 1339A strain created by this introgression retained a 7-Mb B6-derived segment of chromosome 19, encompassing 47.8–54.8 Mb (in the University of California Santa Cruz (UCSC) mm6 genome assembly). The effects of the *T2dm2* locus are more evident in females than in males, so we present the data for only female mice. Obese female mice homozygous for B6 alleles in this segment (1339A^{B6/B6}) had a 30% reduction in 10-week fasting plasma insulin compared to their 1339A^{BT/BT} siblings, which were homozygous for BTBR alleles in the region ($P = 0.009$ for 1339A^{B6/B6} compared to 1339A^{BT/BT}; **Fig. 1a**), replicating the *T2dm2* linkage. The 1339A^{BT/BT} sibs were not significantly different from the BTBR.ob parental population ($P = 0.77$, data not shown). Plasma glucose was 18% higher in 1339A^{B6/B6} mice than in BTBR.ob mice ($P = 0.002$) but was not statistically significant compared with their 1339A^{BT/BT} sibs, consistent with the

¹Departments of Biochemistry, ²Horticulture and ³Statistics, University of Wisconsin-Madison, Madison, Wisconsin 53706, USA. Correspondence should be addressed to A.D.A. (attie@biochem.wisc.edu).

Received 20 December 2005; accepted 6 April 2006; published online 7 May 2006; doi:10.1038/ng1796

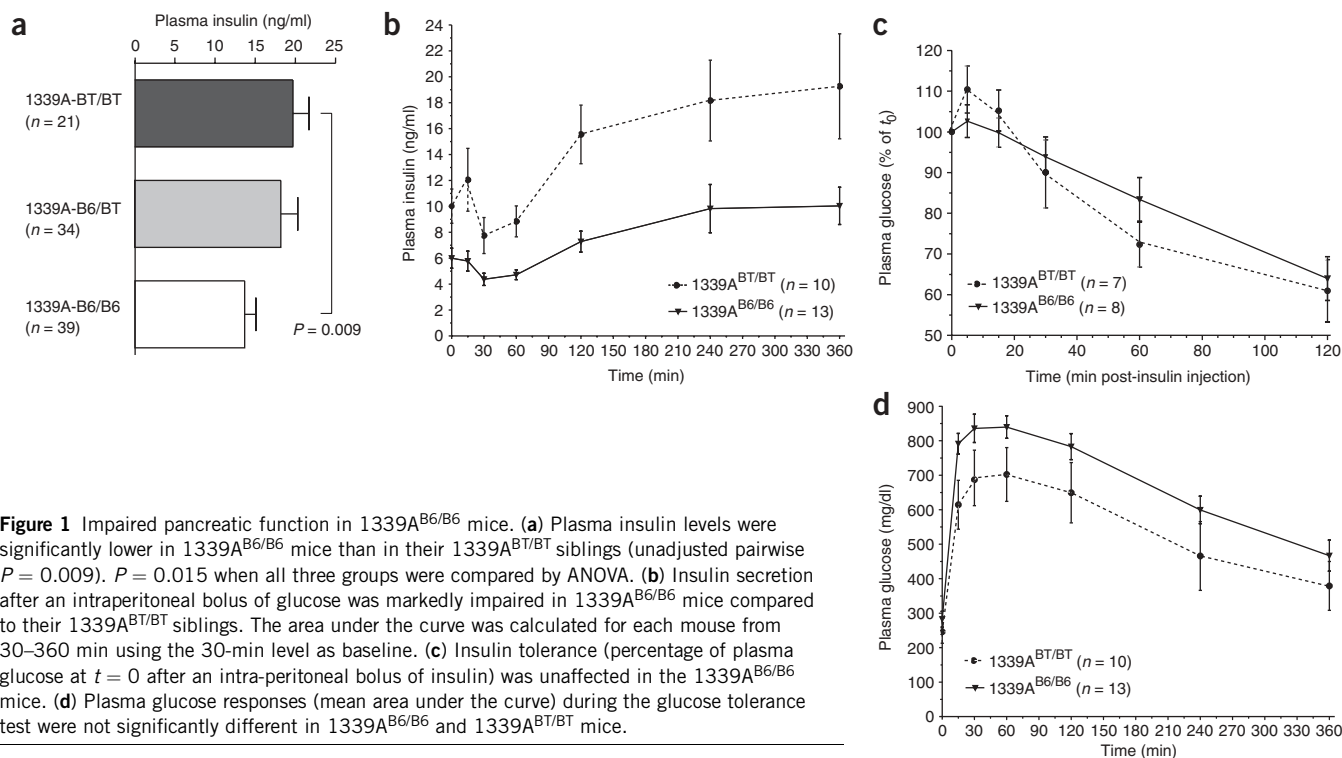


Figure 1 Impaired pancreatic function in 1339A^{B6/B6} mice. **(a)** Plasma insulin levels were significantly lower in 1339A^{B6/B6} mice than in their 1339A^{BT/BT} siblings (unadjusted pairwise $P = 0.009$). $P = 0.015$ when all three groups were compared by ANOVA. **(b)** Insulin secretion after an intraperitoneal bolus of glucose was markedly impaired in 1339A^{B6/B6} mice compared to their 1339A^{BT/BT} siblings. The area under the curve was calculated for each mouse from 30–360 min using the 30-min level as baseline. **(c)** Insulin tolerance (percentage of plasma glucose at $t = 0$ after an intra-peritoneal bolus of insulin) was unaffected in the 1339A^{B6/B6} mice. **(d)** Plasma glucose responses (mean area under the curve) during the glucose tolerance test were not significantly different in 1339A^{B6/B6} and 1339A^{BT/BT} mice.

weaker linkage to plasma glucose levels observed in our F₂ mice¹. Body weight was not significantly different between the mice (**Supplementary Table 1** online), so these effects were not secondary to differences in the degree of obesity of the mice. The 1077 strain, which has an introgressed segment just centromeric to that of the 1339A strain did not have differences in glucose or insulin levels between mice carrying B6 or BTBR alleles of the insert, suggesting that the changes in insulin are specific to the 1339A strain. Thus, allelic differences within this 7-Mb region are sufficient to account for the *T2dm2* QTL.

The most notable phenotype observed in the female 1339A congenic mice was impaired insulin secretion *in vivo*. Plasma insulin levels in response to an intraperitoneal glucose challenge were 50% lower in 1339A^{B6/B6} mice than in their 1339A^{BT/BT} sibs ($P = 0.005$; **Fig. 1b**). In qualitative agreement, fasting C-peptide levels were reduced in 1339A^{B6/B6} mice (**Supplementary Table 1**), although this finding did not reach statistical significance. The C-peptide/insulin ratio was not different between the 1339A^{B6/B6} and 1339A^{BT/BT} mice, consistent with a similar rate of insulin clearance from the circulation in these mice. Furthermore, 1339A^{B6/B6} mice did not have enhanced insulin resistance (**Fig. 1c,d** and **Supplementary Table 1**). We did not observe impaired glucose-stimulated insulin secretion from islets isolated from 1339A^{B6/B6} mice *in vitro*, suggesting that the reduced plasma insulin is specifically related to the ability of the pancreas to secrete insulin in response to a glucose challenge *in vivo*.

Histologically, we observed a broad range of islet morphologies in the congenic mice (**Fig. 2**). Severely disrupted islets (category V) were prevalent in sections from 1339A^{B6/B6} mice, whereas they were observed less often

in sections from 1339A^{BT/BT} mice. Compared to their 1339A^{BT/BT} siblings, 1339A^{B6/B6} mice showed less evidence of morphologically intact islets (category I), although some mouse-to-mouse variation was noted. Thus, the defect in insulin secretion *in vivo* may result from the loss of islet structural integrity.

We refined the location of the gene underlying the *T2dm2* locus by creating a series of 11 subcongenic strains from recombinants of the 1339A strain (**Fig. 3**). The phenotypic effects of *T2dm2* are subtle and thus require large numbers of obese females for detection. To increase our statistical power and ability to detect small effects in the face of high variability, we developed a method to refine the localization of the QTL using data from all strains simultaneously. Subcongenic strains differed by insert genotypes (B6/B6, B6/BT, BT/BT), and rare recombinants were found within some subcongenic strains. We thus used a QTL mapping strategy across our smaller-scale region, exploiting both strain differences in genotype and recombination within strains.

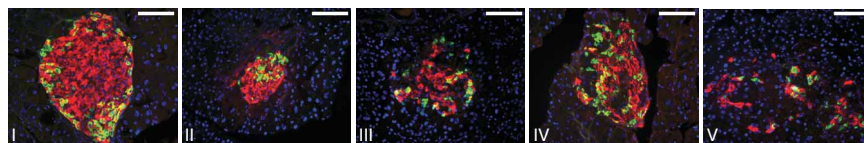


Figure 2 Disrupted islet morphology in 1339A^{B6/B6} mice. Shown are representative images of the broad range of islet morphologies observed in 1339A^{B6/B6} mice. Normal, apparently healthy islets with dense insulin-positive (red) cells in the central core, surrounded by glucagon- and somatostatin-staining (green) cells on the outer edges of the islet (category I), were rare in these mice. The intermediate categories were frequently observed and characterized by the infiltration of glucagon- and somatostatin-positive cells into the center of the islet (category II); the appearance of 'holes' or a loss of insulin staining in the core of the islet, indicated by the presence of blue staining for cell nuclei and absence of red or green staining (category III); or both invasion of non- β cells and the presence of holes (category IV). The most severely disrupted islets (category V) had very few insulin-staining cells in the core and sporadic glucagon- and somatostatin-positive cells, and were observed more often in 1339A^{B6/B6} mice than in their 1339A^{BT/BT} siblings. Scale bars represent 100 μ m.

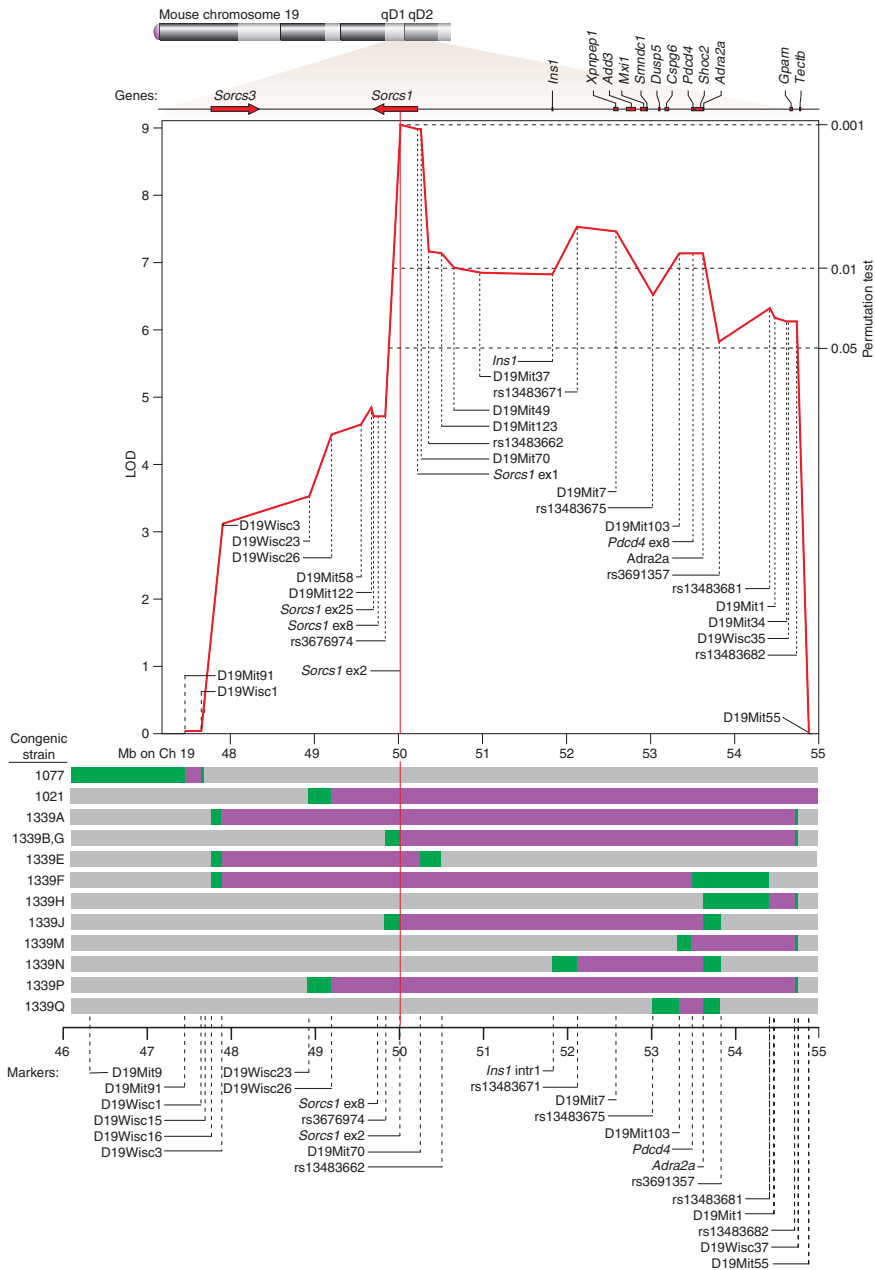


Figure 3 Refinement of the *T2dm2* QTL location with interval-specific congenic mouse strains. Top, genomic region and marker regression meta-analysis of the chromosome 19 region containing the *T2dm2* QTL; bottom, locations of the congenic strains. We localized *T2dm2* to the 7-Mb region contained in the 1339A strain, whereas no phenotypic differences were observed in the 1077 strain. The genes located in this region are indicated at the top of the figure. The remaining 1339 subcongenic strains (shown below the 1339A strain) were derived from recombinants of the 1339A strain. Grey areas (bottom) represent BTBR alleles, whereas purple regions indicate B6 alleles. Alleles residing between adjacent markers typed as B6 and BTBR are undetermined (green). The markers defining these boundaries are shown at the bottom of the figure. The x-axis coordinates are Mb positions based on the March 2005 UCSC mouse genome assembly, which is based on NCBI build 34. The middle panel shows the markers included in the marker regression meta-analysis and the lod score at each position, with horizontal dashed lines indicating the empirical $P < 0.05$, $P < 0.01$ and $P < 0.001$ levels based on permutation tests. A peak lod of 9.05 was obtained in an approximately 242-kb region encompassing the proximal promoter and first exon of the *Sorcs1* gene (from the end of intron 1 to D19Mit70), localizing the *T2dm2* QTL to this region. The lod score at adjacent markers dropped sharply, and no evidence of a second QTL was detected, suggesting that the genetic variation underlying *T2dm2* resides below this peak.

adjacent marker on the centromeric side was a SNP at the end of intron 5 of *Sorcs1* (rs3676974), where the lod score dropped by 4.3 (**Fig. 3**). On the telomeric side, the adjacent SNP (~135 kb telomeric to the transcription start site; rs13483662) showed a lod drop of 1.8. This high level of resolution was made possible on the centromeric side by independent recombination in strains 1339B and 1339G (1339J derived from a recombination in the 1339B strain) and on the telomeric side by the breakpoint of strain 1339E, which

occurs between D19Mit70 and rs13483662 (**Fig. 3**). A large number of mice with the B6/B6 genotype at the peak marker also inherited B6 alleles throughout most of the telomeric side of the region (mice from strains 1339A, B, F, G, J, P and 1021); these mice contributed to the linkage signal, so the lod score did not drop as sharply on this side.

Congenic strains may harbor multiple closely linked genes that each affect the trait of interest and thus increase the likelihood of detecting the region in a genome scan. When we assessed the effects of all pairwise combinations of markers and their interactions, we found no evidence of a second QTL in addition to the one at ~50 Mb ($P > 0.75$ by permutation test). Thus, these data suggest that the differences in plasma insulin result from a single QTL that is most likely to reside under the narrow peak at 50 Mb. As this 242-kb region contains only part of a single known gene, these data strongly suggest that variation within the *Sorcs1* gene underlies *T2dm2*.

We used marker regression to analyze the effects of genotype on plasma insulin levels across all 13 congenic and subcongenic strains, not including any parental BTBR.ob mice. This analysis compared mean log-transformed insulin levels from all 325 obese females, grouped by their marker genotype for each of the 31 microsatellites and single-nucleotide polymorphisms (SNPs) in the region (**Fig. 3**), and assessed significance by permutation testing. To account for any strain-specific effects, we included strain as an interacting covariate in the analysis. We identified a narrow linkage peak (lod = 9.05; $P = 0.001$ by permutation test; **Fig. 3**) where homozygosity for B6 alleles reduced insulin by ~35% (10.7 ± 1.1 ng/ml for B6/B6 mice compared to 16.6 ± 1.1 ng/ml for BT/BT mice at the peak marker, a SNP 205 bp before the start of exon 2).

The lod peak spanned a single exon of just one gene, *Sorcs1*, and encompassed ~242 kb from a SNP at the end of intron 1 to D19Mit70 (~40 kb telomeric to the transcription start site). The

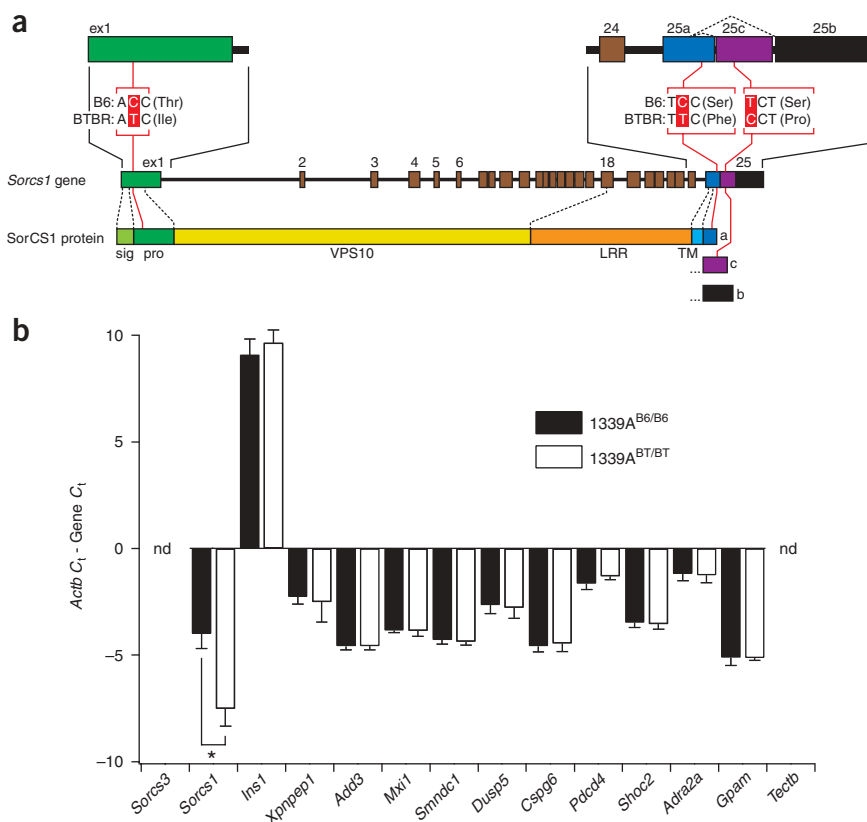


Figure 4 *Sorcs1* coding mutations and expression differences. **(a)** Genetic and corresponding protein structure of *Sorcs1*. The SorCS1 protein is composed of a signal peptide (sig), a propeptide (pro) cleaved by furin, the large VPS10 domain, a leucine-rich repeat (LRR) domain, a single transmembrane domain (TM), and three possible cytoplasmic tails (a–c) arising from alternative splicing of the last exons. Three amino acid differences were detected between B6 and BTBR: a threonine-to-isoleucine variant at amino acid 52 in the propeptide (C172T in the cDNA), a serine-to-phenylalanine variant at amino acid 1140 in the SorCS1a isoform (C3433T in the *Sorcs1a* cDNA) and a serine-to-proline variant at amino acid 1150 in the SorCS1c isoform (T3462C in the *Sorcs1c* cDNA). **(b)** Expression levels of genes in the 7-Mb region in islets from 1339A^{B6/B6} and 1339A^{BT/BT} mice. mRNA expression levels were determined by quantitative RT-PCR for each gene in the region and for β -actin (*Actb*) from 1339A^{B6/B6} ($n = 7$) and 1339A^{BT/BT} ($n = 5$) mice. Expression levels are presented as change in C_t , or the cycle number of each gene subtracted from the cycle number of β -actin for the same cDNA sample. Larger numbers thus correspond to higher expression. nd, expression not detected in islets. *, $P = 0.00001$.

SorCS1 belongs to a family of five proteins (sortilin, SorLA and SorCS1–3) that contain a vacuolar protein sorting-10 (VPS10) domain¹⁰. The SorCS family is distinguished

by the presence of a leucine-rich repeat between the VPS10 and transmembrane domains, which is followed by a short cytoplasmic tail (Fig. 4a). *Sorcs1* is highly expressed in the brain, heart and kidney⁹. It is also expressed in pancreatic islets, in the INS-1 and Min6 β -cell lines (Fig. 4b and data not shown) and at low levels in other tissues⁹.

The reduced insulin levels in the 1339A mice are the result of decreased insulin secretion *in vivo*, which is associated with disrupted islet morphology. The cellular function of SorCS1 is unknown, but it binds to platelet derived growth factor-BB¹¹. This growth factor is required for the recruitment of pericytes or their precursors to vascular endothelial cells, where they stabilize the microvasculature and have a key role in blood vessel development^{12,13}. Maintenance of proper islet vasculature and its expansion during islet growth is important for both insulin secretion and islet survival^{14,15} and may thus be of particular relevance to the phenotype of our mice.

Proteins of the mammalian VPS10 family are synthesized as proproteins and processed to their mature form by furin. The 242-kb *T2dm2* QTL contains a coding mutation in the propeptide of *Sorcs1*. Propeptide binding of sortilin and SorLA has been suggested to prevent premature interaction with their ligands^{16,17}. Propeptide cleavage is crucial for the proper trafficking of sortilin, but it is not required for trafficking of or binding of ligands to SorCS3 (refs. 18,19). The biological role of the SorCS1 propeptide, which binds to mature SorCS1 with low affinity⁹, is not yet known, although it may have a role in modulating SorCS1 function. Alternatively, the phenotype linked to *T2dm2* may be caused by the large difference in *Sorcs1* expression in the islets.

Using a mouse model that mimics common obesity-associated diabetes, we have identified *Sorcs1* as the gene underlying the *T2dm2* locus. These findings provide insight into a process that may

Sorcs1 is the only known gene in the original 7-Mb introgressed chromosomal segment with mutations that affect the protein coding sequence (Supplementary Table 2 online). The 242-kb segment underlying *T2dm2* contains a threonine-to-isoleucine substitution at amino acid 52 (Fig. 4a). Differential splicing of the last exons of *Sorcs1* produces at least three possible isoforms, resulting in proteins that are identical except for their cytoplasmic tails. Outside the QTL region, we detected two additional coding variants that are unique to individual isoforms: a serine-to-phenylalanine substitution at amino acid 1140 of SorCS1a and a serine-to-proline substitution at amino acid 1150 of SorCS1c (Fig. 4a). We also detected several SNPs in the promoter and first intron of *Sorcs1* within the QTL region (Supplementary Table 2).

Given the numerous potential regulatory SNPs that we detected, we assessed whether there were significant differences in *Sorcs1* mRNA levels between 1339A^{B6/B6} and 1339A^{BT/BT} mice. *Sorcs1* was expressed in islets and was expressed at ~10-fold higher levels in 1339A^{B6/B6} mice than in their 1339A^{BT/BT} siblings ($n = 5$ and 7, respectively; $P = 0.00001$; Fig. 4b), as assessed by quantitative RT-PCR. These findings were reproduced by TaqMan analysis of gene expression (data not shown). *Sorcs1* is highly expressed in the brain and is also expressed in the kidney⁹; quantitative RT-PCR on samples from the same 1339A^{B6/B6} and 1339A^{BT/BT} mice did not detect any differences in expression in these tissues. In addition, we did not detect any differences in mRNA levels of any of the other genes in the region in islets, liver or brain (Fig. 4b and Supplementary Table 2), although we cannot formally exclude the possibility that SNPs in our 242-kb region alter *Sorcs1* expression in other tissues or affect the expression of a neighboring gene under other specific temporal or spatial conditions. However, the promoters of the nearest genes are >1.5 Mb from our region, so it is unlikely that SNPs within this region alter gene expression at such extended distances.

be impaired in individuals who are unable to increase or maintain sufficient β -cell mass and insulin secretion to compensate for insulin resistance. A number of rodent and human linkages to type 2 diabetes mellitus-related traits have been mapped to regions containing the *Sorcs1* gene^{20–25}, raising the possibility that this gene has broad relevance to the development of type 2 diabetes mellitus.

METHODS

Creation of congenic mice. After initial selection of F₂ mice with B6 alleles on chromosome 19, congenic mice were developed by at least five rounds of marker-assisted backcrossing into BTBR (such that no remaining B6 alleles were detected outside their chromosome 19 region) and subsequent breeding to BTBR.ob mice. The 1339A line inherited an approximately 7-Mb region of the B6 genome; the rest of the genome is BTBR. The 1077 strain inherited an approximately 1.3-Mb nonoverlapping region centromeric to that of the 1339A strain. Subcongenic strains ($n = 11$) were bred from recombinants of the 1339A strain after an initial backcross to BTBR.ob to separate the recombinant and nonrecombinant alleles. All strains were maintained by a combination of heterozygous and homozygous sibling breeding pairs within each strain.

Passenger loci—regions of the donor genome linked to the targeted region that remain because of double recombination events—were excluded using publicly available SNP data from the Wellcome Trust Centre for Human Genetics and the Mouse Phenome Database and by our own genotyping. We obtained genotypes for the B6 and BTBR strains at approximately 400 markers on chromosome 19. From this data, we identified several haplotype blocks where the B6 and BTBR strains did not differ. The largest of these spanned 0–16, 32–35 and 37–44 Mb (UCSC mm6 assembly), although several smaller blocks were also observed. In regions where the genomes differed, we examined markers at a maximum spacing of one marker per Mb ($n = 23$ markers total), and we did not detect any residual B6 alleles in the 1339A strain. The chance that a double recombination event occurred and resulted in passenger loci between any pair of these markers is very small.

Animal procedures. Mice were housed in an environmentally controlled facility (12-hour light and dark cycles) with free access to food (5008; Purina) and water. Mice were fasted from approximately 8 AM until noon before blood collection for plasma glucose, insulin, triglyceride and C-peptide measurements at 10 weeks of age, and before being killed at 14 weeks of age. Plasma glucose levels were measured using a commercially available kit (994-90902; Wako Chemicals). Plasma insulin, glucagon (14 weeks) and C-peptide levels were assayed using radioimmunoassays (RI-13K, GL-32K and RCP-21K, respectively; Linco Research).

Glucose tolerance tests were performed on 11-week-old mice fasted overnight (6 PM–9 AM). Glucose (2 mg per g of body weight in sterile saline) was administered intraperitoneally. Blood samples (<50 μ l) were drawn before glucose injection and at 15, 30, 60, 120, 240 and 360 min after injection for glucose and insulin measurements. Insulin tolerance tests were performed on 12-week-old mice beginning between 1 PM and 2 PM on nonfasting animals. Blood samples were drawn before insulin injection (20 milliunits per g body weight in sterile saline; Humulin R, HI-210; Eli Lilly) and at 5, 15, 30, 60 and 120 min after injection for glucose and insulin measurements. Animals were allowed free access to water, but food was removed from the cages during both of these tests.

For determination of whole-pancreas insulin and glucagon content, pancreata were immediately removed and placed in 4 ml of ice-cold acid ethanol. After being weighed, the samples were manually minced and allowed to extract at -20°C for a minimum of 18 h. After neutralization with 10 N NaOH, cellular debris was removed by centrifugation for 5 min at 1,000g at 4°C . The supernatant was removed and diluted 1:10,000 for the insulin and glucagon measurements described above. Islets were isolated, and insulin secretion studies at 1.7 and 16.7 mM glucose were performed as previously described²⁶.

All animal procedures were approved by the University of Wisconsin Animal Care and Use Committee.

Islet immunofluorescence. Pancreata were removed and fixed in freshly made 4% paraformaldehyde at 4°C overnight. Samples were then infiltrated with

30% sucrose at 4°C overnight and embedded in Neg50 freezing medium (Richard-Allan Scientific). Cryosections (10 μ m) were obtained from several positions throughout the pancreas, at a minimum distance of 450 μ m between sections, and stored at -20°C until staining. Multiple sections from two 1339A^{BT/BT} and three 1339A^{B6/B6} mice were examined.

For staining, slides were removed from -20°C storage and placed into PBS for 10 min. Sections were blocked with 10% donkey serum (Jackson ImmunoResearch) in PBS for 30 min and then washed with PBS. Guinea pig antibody to insulin (1:500; I-8510; Sigma), mouse antibody to glucagon (1:100; G-2654; Sigma) and goat antibody to somatostatin (1:100; SC-7819; Santa Cruz Biotechnology) were added and incubated at 4°C overnight. Slides were washed with PBS before the addition of Cy3-conjugated donkey anti-guinea pig (1:500; 706-165-148; Jackson ImmunoResearch), FITC-conjugated donkey anti-mouse (1:200; 715-095-150; Jackson ImmunoResearch) and Alexa Fluor 488-conjugated donkey anti-goat (1:200; A-11055; Invitrogen) secondary antibodies. The slides were then incubated in the dark for 30 min at room temperature, washed with PBS and allowed to air-dry in the dark. Staining was preserved and nuclei identified by adding a drop of Vectashield with DAPI (H-1200; Vector Labs) to each tissue section before the addition of a cover slip. Using this procedure, insulin was stained red, glucagon and somatostatin were both stained green and nuclei were stained blue. Images were acquired by IP Lab software (Scanalytics).

Mouse genotyping. Genotyping of microsatellite markers (Invitrogen) was performed by standard techniques¹, with visualization of SYBR Green-stained (Cambrex BioScience) PCR products on 8% polyacrylamide gels. B6, BTBR and F₁ (heterozygous) DNA were included on each gel for comparison. In areas where no known polymorphic markers existed, we identified long di- or trinucleotide repeats in the genomic sequence and designed primers to amplify these regions. Those that were polymorphic between the B6 and BTBR strains and that were included in our analysis are named D19WiscX (primer sequences given in **Supplementary Table 3** online). SNP markers identified from the SNPview public mouse SNP database are referred to by their RefSNP (rs) accession numbers and were verified to be polymorphic by sequencing the B6 and BTBR strains or were identified from our sequencing efforts and are located in or immediately adjacent to *Sorcs1* exons 1, 2, 8 and 25; the *Ins1* promoter; *Pdcd4* exon 8; and the *Adra2a* promoter. Subsequent genotyping of these SNPs was done either by sequencing or by restriction fragment-length polymorphism analysis; primer sequences are given in **Supplementary Table 3**.

Sequence and gene expression analysis. The genomic sequence of each gene from the B6 strain was obtained from the UCSC mouse genome assembly, and primers (**Supplementary Table 3**) were designed to amplify each exon plus at least 50 nucleotides of the adjacent introns. We also analyzed a minimum of 200 nucleotides of the proximal promoter (often >1 kb). These fragments were amplified from the BTBR strain. Purified PCR products were subjected to thermocycle sequencing, and the resulting fragments were analyzed on capillary-based machines by the University of Wisconsin Biotechnology Center DNA Sequence Laboratory. Sequence analysis was done by aligning the sequence to the genomic B6 sequence (Staden Package version 4.6 or Sequencher version 4.1.4, GeneCodes Technology). All exonic changes were verified by resequencing both the BTBR and B6 strains.

RNA was extracted from flash-frozen brains, livers and kidneys of 14-week-old 1339A^{B6/B6} and 1339A^{BT/BT} mice using RNeasy kits (Qiagen) after treatment with RNAlater Ice (Ambion) to prevent degradation, according to the manufacturer's directions. RNA was extracted from 1339A^{B6/B6} and 1339A^{BT/BT} islets that were isolated as described above, hand-picked under a stereomicroscope to remove contaminating acinar tissue, immediately homogenized in 0.35 ml of RLT buffer (Invitrogen) and stored at -20°C . RNA was purified using RNeasy-mini columns (Qiagen) according to the manufacturer's directions. An Agilent Bioanalyzer 2100 was used to assess RNA quality for all samples, which typically showed a 28/18S ratio of ~ 1.5 or greater.

Gene expression was quantitatively measured using a 7500 fast real-time PCR system (Applied Biosystems). cDNA was synthesized from 1 μ g of total RNA using the SuperScriptIII first-strand cDNA synthesis kit (Invitrogen) primed with a mixture of oligo-dT and random hexamers. Primers (specified in

Supplementary Table 3) were obtained from Integrated DNA Technologies. The SYBR Green PCR core reagent kit (Applied Biosystems) was used to determine relative expression. TaqMan probes (Applied Biosystems) were used to confirm the differential expression of *Sorcs1* in islets. *Sorcs1* (Mm00491259) and *Actb* (Mm0060793) probes and the TaqMan Universal PCR master mix were obtained from Applied Biosystems and used according to the manufacturer's instructions. The housekeeping gene *Actb* was used as a normalization control.

Statistical analysis. Plasma insulin values were log-transformed before analysis, although the untransformed data are presented for easier interpretation. The areas under the curves for the glucose and insulin levels during the glucose tolerance test were calculated by integration using the trapezoidal rule, from the baseline at $t = 0$ to 360 min and from the baseline at $t = 30$ min to 360 min, respectively. Statistical analysis of the phenotypic parameters in the 1339A mice (as shown in **Supplementary Table 1**) was done by ANOVA. Because of the number of comparisons in this data set, a conservative Bonferroni correction indicates that the appropriate significance threshold is $P < 0.006$. Statistics on these data were analyzed with Prism software version 4.02 (Graph Pad Software).

We developed a meta-analysis method to combine QTL gene-mapping information across closely related interval-specific congenic mouse strains. For our fine mapping of 10-week log-transformed insulin values in the obese mice, we extended the methods for QTL mapping^{27,28} by allowing for strain differences. That is, we used marker regression using the scanone algorithm in the R/qtl package²⁹, with strain as an interacting covariate. At each marker, we excluded the few animals with missing genotypes, although the results were essentially unchanged if missing marker genotypes (2.4%) were inferred with the Viterbi algorithm. The analysis accounts for differences between strains to allow testing for the genotypic effect of one QTL. Formal evaluation of QTL involved extending the scanone permutation test³⁰ to allow for strain effects. Thus, we separately permuted the phenotypes among individuals within each strain and computed the maximum lod across all markers in the region. Empirically, this increased the noise in estimating permutation-based quantiles. We therefore used 5,000 permutations, rather than the originally recommended 1,000, to determine P values. We tested for evidence of a second QTL (with or without epistasis) using the R/qtl scantwo routine, again with an extension to the permutation test to allow for strain effects. Our initial analysis included both males and females ($n = 595$) and included sex in the model, but as the evidence was much weaker in males, the analysis presented here is for females only ($n = 325$).

Accession codes. GenBank GeneIDs: *Sorcs3*, 66673; *Sorcs1*, 58178; *Ins1*, 16333; *Xpnp1*, 170750; *Add3*, 27360; *Mxi1*, 17859; *Snmnd1*, 76479; *Dusp5*, 240672; *Cspg6*, 13006; *Pdcd4*, 18569; *Shoc2*, 56392; *Adra2a*, 11551; *Gpam*, 14732; *Tectb*, 21684. All BTBR genomic sequences have been deposited to GenBank under accession numbers DQ479917–DQ479930.

URLs. The Wellcome Trust Centre for Human Genetics is available at <http://zeon.well.ox.ac.uk/rmott-bin/strains.cgi>. The Mouse Phenome Database is available at <http://aretha.jax.org/pub/cgi/phenome/mpdcgi?rt=snp>. The SNPview database is available at <http://snp.gnf.org/GNF10K/>. RefSNP accession numbers are available at <http://www.ncbi.nlm.nih.gov/projects/SNP>. The UCSC genome assembly is available at <http://www.genome.ucsc.edu/>.

Note: Supplementary information is available on the Nature Genetics website.

ACKNOWLEDGMENTS

This work was supported by US National Institute of Diabetes and Digestive and Kidney Diseases grants 58037 and 66369 to A.D.A.; American Heart Association postdoctoral fellowships 0325480Z and 0525688Z to S.M.C.; grants from the US Department of Agriculture's Cooperative State Research, Education and Extension Service to B.S.Y. and A.D.A.; a Sponsored Research Agreement with Xenon Pharmaceuticals (formerly Xenon Genetics) and an American Diabetes Association Mentor-Based Fellowship to A.D.A. We thank W.F. Dove for his advice and encouragement throughout this project, A. Steinberg for his expert assistance in preparing the figures for this manuscript and the staff in our animal care facility for their dedication to this work.

COMPETING INTERESTS STATEMENT

The authors declare that they have no competing financial interests.

Published online at <http://www.nature.com/naturegenetics>

Reprints and permissions information is available online at <http://npg.nature.com/reprintsandpermissions/>

1. Stoehr, J.P. *et al.* Genetic obesity unmasks nonlinear interactions between murine type 2 diabetes susceptibility loci. *Diabetes* **49**, 1946–1954 (2000).
2. Bell, G.I. & Polonsky, K.S. Diabetes mellitus and genetically programmed defects in beta-cell function. *Nature* **414**, 788–791 (2001).
3. Rhodes, C.J. Type 2 diabetes—a matter of beta-cell life and death? *Science* **307**, 380–384 (2005).
4. Florez, J.C., Hirschhorn, J. & Altshuler, D. The inherited basis of diabetes mellitus: implications for the genetic analysis of complex traits. *Annu. Rev. Genomics Hum. Genet.* **4**, 257–291 (2003).
5. Permutt, M.A., Wasson, J. & Cox, N. Genetic epidemiology of diabetes. *J. Clin. Invest.* **115**, 1431–1439 (2005).
6. Parikh, H. & Groop, L. Candidate genes for type 2 diabetes. *Rev. Endocr. Metab. Disord.* **5**, 151–176 (2004).
7. Barroso, I. *et al.* Candidate gene association study in type 2 diabetes indicates a role for genes involved in beta-cell function as well as insulin action. *PLoS Biol.* **1**, E20 (2003).
8. Clee, S.M., Nadler, S.T. & Attie, A.D. Genetic and genomic studies of the BTBR ob/ob mouse model of type 2 diabetes. *Am. J. Ther.* **12**, 491–498 (2005).
9. Hermey, G. *et al.* Characterization of *Sorcs1*, an alternatively spliced receptor with completely different cytoplasmic domains that mediate different trafficking in cells. *J. Biol. Chem.* **278**, 7390–7396 (2003).
10. Hampe, W., Rezagoui, M., Hermans-Borgmeyer, I. & Schaller, H.C. The genes for the human VPS10 domain-containing receptors are large and contain many small exons. *Hum. Genet.* **108**, 529–536 (2001).
11. Hermey, G., Sjogaard, S., Petersen, C.M., Nykjaer, A. & Gliemann, J. Tumour necrosis factor- α convertase mediates ectodomain shedding of Vps10p-domain receptor family members. *Biochem. J.* **395**, 285–293 (2006).
12. Song, S., Ewald, A.J., Stallcup, W., Werb, Z. & Bergers, G. PDGFR β + perivascular progenitor cells in tumours regulate pericyte differentiation and vascular survival. *Nat. Cell Biol.* **7**, 870–879 (2005).
13. Abramsson, A., Lindblom, P. & Betsholtz, C. Endothelial and nonendothelial sources of PDGF-B regulate pericyte recruitment and influence vascular pattern formation in tumors. *J. Clin. Invest.* **112**, 1142–1151 (2003).
14. Lammert, E. *et al.* Role of VEGF-A in vascularization of pancreatic islets. *Curr. Biol.* **13**, 1070–1074 (2003).
15. Brissova, M. *et al.* Intra-islet endothelial cells contribute to revascularization of transplanted pancreatic islets. *Diabetes* **53**, 1318–1325 (2004).
16. Jacobsen, L. *et al.* Activation and functional characterization of the mosaic receptor SorLA/LR11. *J. Biol. Chem.* **276**, 22788–22796 (2001).
17. Munck Petersen, C. *et al.* Propeptide cleavage conditions sortilin/neurotensin receptor-3 for ligand binding. *EMBO J.* **18**, 595–604 (1999).
18. Westergaard, U.B. *et al.* *Sorcs3* does not require propeptide cleavage to bind nerve growth factor. *FEBS Lett.* **579**, 1172–1176 (2005).
19. Westergaard, U.B. *et al.* Functional organization of the sortilin Vps10p-domain. *J. Biol. Chem.* **279**, 50221–50229 (2004).
20. Duggirala, R. *et al.* Linkage of type 2 diabetes mellitus and of age at onset to a genetic location on chromosome 10q in Mexican Americans. *Am. J. Hum. Genet.* **64**, 1127–1140 (1999).
21. Galli, J. *et al.* Genetic analysis of non-insulin dependent diabetes mellitus in the GK rat. *Nat. Genet.* **12**, 31–37 (1996).
22. Kim, J.H. *et al.* Genetic analysis of a new mouse model for non-insulin-dependent diabetes. *Genomics* **74**, 273–286 (2001).
23. Kluge, R. *et al.* Quantitative trait loci for obesity and insulin resistance (Nob1, Nob2) and their interaction with the leptin receptor allele (LeprA720T/T1044I) in New Zealand obese mice. *Diabetologia* **43**, 1565–1572 (2000).
24. Wiltshire, S. *et al.* A genome-wide scan for loci predisposing to type 2 diabetes in a U.K. population (the Diabetes UK Warren 2 Repository): analysis of 573 pedigrees provides independent replication of a susceptibility locus on chromosome 1q. *Am. J. Hum. Genet.* **69**, 553–569 (2001).
25. Wei, S. *et al.* Mapping and characterization of quantitative trait loci for non-insulin-dependent diabetes mellitus with an improved genetic map in the Otsuka Long-Evans Tokushima fatty rat. *Mamm. Genome* **10**, 249–258 (1999).
26. Rabaglia, M.E. *et al.* Alpha-ketooisocaproate-induced hypersecretion of insulin by islets from diabetes-susceptible mice. *Am. J. Physiol. Endocrinol. Metab.* **289**, E218–E224 (2005).
27. Liu, Y. & Zeng, Z.B. A general mixture model approach for mapping quantitative trait loci from diverse cross designs involving multiple inbred lines. *Genet. Res.* **75**, 345–355 (2000).
28. Zou, F., Yandell, B.S. & Fine, J.P. Statistical issues in the analysis of quantitative traits in combined crosses. *Genetics* **158**, 1339–1346 (2001).
29. Broman, K.W., Wu, H., Sen, S. & Churchill, G.A. R/qtl: QTL mapping in experimental crosses. *Bioinformatics* **19**, 889–890 (2003).
30. Churchill, G.A. & Doerge, R.W. Empirical threshold values for quantitative trait mapping. *Genetics* **138**, 963–971 (1994).